Author's Accepted Manuscript

The performance of affordable and stable cellulose-based poly-ionic membranes in CO_2/N_2 and CO_2/CH_4 gas separation

Daria Nikolaeva, Itxaso Azcune, Marek Tanczyk, Krzysztof Warmuzinski, Manfred Jaschik, Marius Sandru, Paul Inge Dahl, Aratz Genua, Sandrine Lois, Edel Sheridan, Alessio Fuoco, Ivo Vankelecom

www.elsevier.com/locate/memsci

PII: S0376-7388(18)30620-3
DOI: https://doi.org/10.1016/j.memsci.2018.07.057
Reference: MEMSCI16336

To appear in: *Journal of Membrane Science*

Received date: 6 March 2018
Revised date: 11 June 2018
Accepted date: 20 July 2018

Cite this article as: Daria Nikolaeva, Itxaso Azcune, Marek Tanczyk, Krzysztof Warmuzinski, Manfred Jaschik, Marius Sandru, Paul Inge Dahl, Aratz Genua, Sandrine Lois, Edel Sheridan, Alessio Fuoco and Ivo Vankelecom, The performance of affordable and stable cellulose-based poly-ionic membranes in CO_2/N_2 and CO_2/CH_4 gas separation, *Journal of Membrane Science,* https://doi.org/10.1016/j.memsci.2018.07.057

The performance of affordable and stable cellulose-based poly-ionic membranes in CO_2/N_2 and CO_2/CH_4 gas separation

Daria Nikolaeva,[a] Itxaso Azcune,[b] Marek Tanczyk,[c] Krzysztof Warmuzinski,[c] Manfred Jaschik,[c] Marius Sandru,[e] Paul Inge Dahl,[e] Aratz Genua,[b] Sandrine Lois,[d] Edel Sheridan,[e] Alessio Fuoco,[f] Ivo Vankelecom.[a]

[a] Centre for Surface Chemistry and Catalysis, Department Interface-chemistry, Faculty of Bio-engineering Sciences, KU Leuven, Belgium.
[b] Polymers & Composite Unit, IK4-CIDETEC, Donostia- San Sebastián. Spain.
[c] Institute of Chemical Engineering, Polish Academy of Sciences, Gliwice, Poland.
[d] SOLVIONIC, Site Bioparc 195, route dÉspagne, BP1169, 31036 Toulouse Cedex 1, France.
[e] SINTEF, Industry, Trondheim, Norway.
[f] Institute on Membrane Technology (ITM-CNR), Via P. Bucci 17/C, 87036 Rende (CS), Italy.

Abstract

The majority of commercial membrane units for large-scale natural gas sweetening are based on cellulose acetate (CA). However, the low selectivity and risk for and plasticisation affect adversely the performance of CA-based systems. Herein, we present a new class of CA-derived poly(ionic liquid) (PIL) as a thin film composite (TFC) membrane for CO_2 separations. CA is modified with pyrrolidinium cations through alkylation of butyl chloride, substituting the hydroxyl group in the polymer backbone, and further anion exchange to bis(trifluoromethylsulfonyl)imide, P[CA][Tf_2N]. The synthesised PIL material properties are extensively studied. The CO_2 separation performances of the newly synthesised materials is evaluated by gravimetric gas sorption experiments, single gas time-lag experiments on thick membranes, and mixed-gas separation experiments on TFC membranes. The results are compared to the parent material (CA) as well as a reference PIL (poly(diallyldimethyl ammonium) bis(trifluoromethylsulfonyl)imide (P[DADMA][Tf_2N])). The ideal CO_2/N_2 sorption selectivity of P[CA][Tf_2N] is constant up to 10 bar. The single gas transport measurements in P[CA][Tf_2N] reveal improved ideal CO_2 selectivity for the CO_2/N_2 gas pair and increased CO_2 permeability for the CO_2/CH_4 gas pair compared to the reference PIL. Mixed-gas permeation tests demonstrated that P[CA][Tf_2N]-based membranes with a 5 μm thick selective layer has a two-fold higher CO_2 flux compared to conventional CA. These results present CA modification into PILs as a successful approach promoting the higher permeate flows and improved process stability in a wide range of concentrations and pressures of CO_2/N_2 and CO_2/CH_4 gas mixtures.

Key words

Cellulose acetate, poly(ionic liquid), poly(diallyldimethyl ammonium) bis(trifluoromethylsulfonyl)imide (P[DADMA][Tf_2N]), thin-film composite membrane, time-lag, ideal sorption selectivity, gas separation, CO_2 capture, flue gas, biogas.

1. Introduction

Cellulose is an almost inexhaustible bio-based polymeric raw material [1]. Being a linear homopolymer with D-glucose monomers, cellulose exhibits a broad chemical processability that enables the development of new functional materials. Cellulose acetate esters (CA) are the most widely used type of functionalized cellulose. CA is made by reacting the free hydroxyl groups in cellulose with acetic acid or acetic anhydride in the presence of sulphuric acid, followed by the hydrolysis of acetyl groups [2]. CA materials range from cellulose triacetate to materials with different degree of acetylation, defined by the degree of substitution (DS). Importantly, the conversion of cellulose to CA alters the physicochemical properties, improving its solubility in organic solvents and facilitating its processing as an ordinary thermoplastic material. Being a biodegradable, low cost and widely available polymer, CA is widely used in a variety of commercial applications, including films, moulded goods, and fabrics [3]. CA was one of the first materials implemented in membrane technology on a large scale, and has since been used in water purification, medical applications, and gas separation [4].

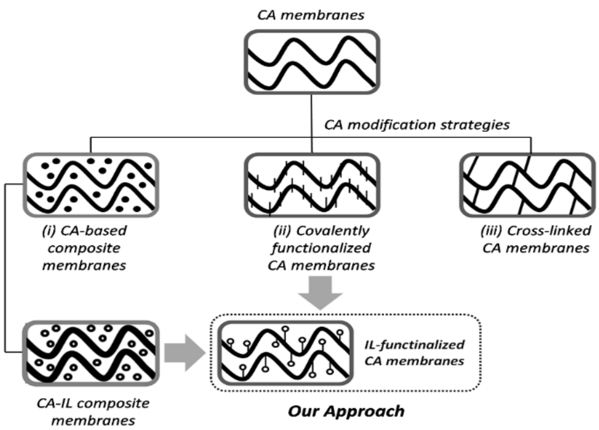

Scheme 1 Pathways to modify cellulose acetate-based membranes

Currently, CA is an industrial standard for the removal of CO_2 from natural gas, and along with other commercially available membranes, such as polyimides, dominates the market of CO_2 separations [5]. Even though newly emerged polymers (*e.g.* thermally rearranged polymers, polymers of intrinsic microporosity and fixed-site-carrier polymers) outperform CA separation performance [6], the interest in developing CA-based membranes persists due to its availability and proven characteristics. Prior research provides ample examples of CA-based materials overcoming existing limitations, such as loss of selectivity under aggressive feed conditions. Scheme 1 **Pathways to modify cellulose acetate-based membranes**

outlines several CA-based materials: (i) mixed matrix membranes (MMM) comprised of 0.1 wt% functionalized multi-walled carbon nanotubes, nanoporous layered silicate AMH-3 embedded into CA matrix, and blend membranes with PEG; (ii) covalently functionalized CA membranes, for example, with adamantine groups; and (iii) cross-linked CA membranes using vinyltrimethoxysilane [7–11]. Additional interest for cellulose chemistry focuses on cellulose solubility and reactivity in ionic liquids (ILs) and their role as a process medium for the CA phase inversion in membrane production [12,13].

In recent years, ionic liquids have demonstrated promising candidates for gas separation purposes [14–16]. Task-specific ILs have been investigated in bulk, supported in porous membranes (SILMs) and blended with membrane polymers to improve gas separation properties [17]. However, the combination of ILs and cellulose derivatives for gas separation purposes has remained virtually unexplored. Pioneering works on the CA doped with imidazolium based ILs [1-ethyl-3-methylimidazolium][BF4] and [1-ethyl-3-methylimidazolium][DCA] [18], ether- or alkyl-functionalized pyridinium based ILs [E_nPy][Tf_2N] and [C_nPy][Tf_2N] indicate that CA composite membranes with ILs show high selectivies and permeability in gas separation technologies [19], however the ILs are very prone to leaching and cannot provide a stable separation performance.

Polymers constituted by IL monomers, or simply poly(ionic liquids) (PILs), combine the physicochemical affinity towards CO_2, featured by ILs, with the robust mechanical properties inherent to polymers [20,21]. PILs have been evaluated not only as neat materials, but also blended with ILs into composite materials. In these blends, PILs prevent the system phase separation and ILs leaching under pressure, while maintaining the overall performance, as strong ionic interactions are created between the free ILs and the ionic side chains of the PIL backbone [22]. Accordingly, the preparation of a CA-based PILs membrane offers the opportunity to make an affordable, stable membrane with unique separation properties.

The combination of cellulose/PILs-like materials can provide a variety of interesting materials [23,24], however their function in application has yet to be determined especially including the gas separation. The latter is surprising, as in gas separation PILs provide additional advantages like improved CO_2 permeabilities and selectivity stability in humidified streams. The functionalization of polymers with ionic moieties may lead to favourable synergies for CO_2 separation, as observed for polybenzimidazoles in terms of permselectivity [25]. Additionally, the positive influence of water vapour on the gas permeability of PIL membranes has been reported recently [26]. Under humid conditions, both, the CO_2 and CH_4 permeabilities increased with no negative impact on selectivity.

In present paper the gas separation benefits of functionalizing CA with ionic functionalities are studied. The synthesis and characterization of CA-derived PIL-like polymers is described by covalent grafting of pyrrolidinium moieties to the free hydroxyl groups of commercially available CA, followed by anion metathesis. Gas sorption and permeability to single gases of the new polymer (P[CA][Tf_2N]) were assessed and compared to the parent material and a reference PIL, poly(diallyldimethylammonium Tf_2N) (P[DADMA][Tf_2N]). Thin film composite (TFC) membranes were prepared from studied materials and their separation performance was examined in a series of experiments with a range of concentrations and pressures of CO_2/N_2 and CO_2/CH_4 gas mixtures.

2. Experimental

1.1. Materials

Cellulose acetate (39.7 wt% acetyl content, $\overline{M}_n = 50$ kDa), poly(diallyldimethyl ammonium) chloride (20 wt% in water, $\overline{M}_w = 200 - 350$ kDa), *N*-methylpyrrolidine (> 99 %), and triethylamine (99 %) were purchased from Sigma-Aldrich. The CA powder was dried under vacuum at 100 °C for 48 h to remove adsorbed moisture before use. 4-Chlorobutyryl chloride (98 %) was purchased from Acros Organics. Dichloromethane (99.5 %) was purchased from Scharlab. Bis(trifluoromethylsulfonyl)imide lithium salt ($LiTf_2N$) was purchased from IoLiTec. *p*-Xylylenediamine (XDA, > 98%) cross-linker was purchased from Fluka. *N*-methylpyrrolidinone (NMP, Acros, 99 %), tetrahydrofurane (THF, Acros, 99.5 %), acetone (Merck, 99.8 %), ethanol (EtOH, Fisher Scientific, 99.5 %), isopropanol (IPA, VWR, 99.5 %), methanol (Acros, 99.8 %), and ethyl acetate (VWR, 99.9 %) were used as solvents without further purification. Matrimid® 9725 was kindly provided by Huntsman (Switzerland). The non-woven polypropylene/polyethylene (PP/PE) fabric Novatexx® 2483 was supplied by Freudenberg (Germany).

1.2. Polymer synthesis

Synthesis of poly(diallyldimethyl ammonium) bis(trifluoromethylsulfonyl)imide (P[DADMA][Tf_2N]).

Poly(diallyldimethyl ammonium) chloride (0.88 mol, 709 g) was diluted with water (709 g) and added to the solution of $LiTf_2N$ (0.98 mol, 373 g, 75 % in water) in 142 g of water. The mixture was stirred during 48 hours. After filtration, washing and drying, a white solid was obtained (295 g, 74 % yield).

Synthesis of CA-based pyrrolidinium derivatized poly(ionic liquid) (P[CA][Tf_2N]).

Dried CA (121.9 mmol, 30 g) was dispersed in dry dichloromethane (350 mL), and triethylamine (231.6 mmol, 32.3 mL) was added. The mixture was vigorously stirred until complete dissolution of the polymer. The solution was then cooled to 0 °C and 4-chlorobutyryl chloride (182.9 mmol, 20.9 mL) was introduced dropwise. The reaction mixture was stirred at ambient temperature for 24 h, subsequently centrifuged to remove the salt, and finally concentrated in the rotary evaporator. The product was dissolved in acetone and precipitated in aqueous ethanol solution (EtOH:H_2O, 4:1, 450 mL) to remove salts and excess reagents. The intermediate product, namely P-CA. was filtrated and dried under reduced pressure, yielding 29.7 g (50 %) of a white powder.

To the CA-P solution (20.3 mmol, 13 g) in DMF (150 mL) at 80 °C, *N*-methylpyrrolidinium (61.0 mmol, 6.5 mL) was added dropwise. After being stirred for 3 days, the corresponding PIL (P[CA][Cl]) was precipitated and washed with ethyl acetate. For the anion exchange, the precursor P[CA][Cl] was dissolved in water and a solution of $LiTf_2N$ salt (20.3 mmol, 5.8 g) was added dropwise and stirred for 24 h. The final product (P[CA][Tf_2N]) was collected by filtration in the form of white solid. The obtained product was washed with deionised water until the test with $AgNO_3$ was negative and no halide anions could be identified, filtered and dried until constant weight (yield 12 g, 82 %). An overview of this chemical synthesis route is reported in Scheme 2 **Post-synthetic conversion of CA into P[CA][Tf2N] through IL sites incorporation and subsequent anion metathesis.**

.

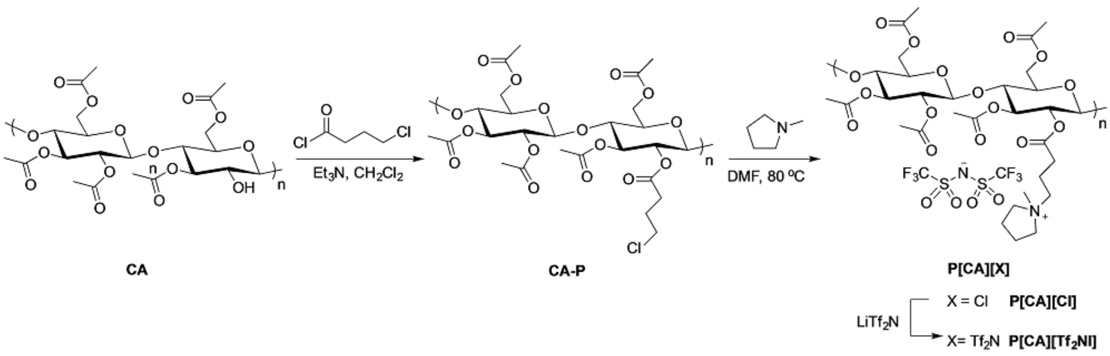

Scheme 2 Post-synthetic conversion of CA into P[CA][Tf_2N] through IL sites incorporation and subsequent anion metathesis.

1.3. Material characterisation

The FTIR spectra of the polymers were recorded with an ATR-FTIR Jasco 4100 spectrometer (4000-400 cm^{-1}, 4 cm^{-1} resolution, and the total number of 16 scans). The NMR spectra were measured on a Bruker Avance III 500 MHz (^1H) NMR spectrometer using deuterated dimethylsulfoxide (DMSO-d6) as solvent. Thermo-gravimetric analyses (TGA) were performed using a Q500 TG-DTA analyser (TA Instruments) between 25 and 700 °C, under air atmosphere and a heating rate of 10 °C·min^{-1}. Differential scanning calorimetry (DSC) analyses were performed on Pyris Diamond DSC (Perkin-Elmer) from ambient temperature to 230 °C. The glass transition temperature (T_g) was obtained as the inflection point of the heat flow step (2nd heat), recorded at a scan rate of 20 °C·min^{-1}. The melting point and the enthalpy for indium (m_p 156.6 °C, ΔH_m 28.5 J·g^{-1}) was used for the temperature and the heat capacity calibration.

Sorption analysis. N_2 and CO_2 sorption isotherms were obtained at 20 °C using a gravimetric analyser (Hiden Isochema IGA-003). The chosen experimental pressure range was 0-5 bar for P[DADMA][Tf_2N] and 0-10 bar for CA and P[CA][Tf_2N]. Powdery samples were degassed under vacuum at a temperature of 70 °C (CA, P[DADMA][Tf_2N]) and 20 °C (P[CA][Tf_2N]) before the measurements. The time required to obtain each experimental value equalled 120 min for CA and 360 min for PIL-based samples.

1.4. Membrane preparation

Thick dense films.

The neat polymeric membranes were prepared by a solution casting method reported previously [27]. The casting solution contained 8 wt% of polymer in acetone. After homogenisation and de-gassing, the polymer solution (2 mL) was cast onto a polyester film firmly fixed to the stainless steel frame (∅50 mm) in a controlled environment at 25 ± 1 ºC and 20 ± 1 % relative humidity (RH). The polymeric film was left to dry for ca. 72 h. The dry membranes were removed from the frame and peeled of the support. The membranes were additionally dried in the vacuum chamber for 3 h prior the measurements.

Thin film composites.

Polymeric supports were prepared by a phase inversion method from commercially available polyimide (PI) according to the method described previously [28–30]. The casting solution was prepared in the mixture of solvents 62.25/20.75/2.00 wt % of NMP/THF/H_2O with 15 wt % Matrimid® 9725. After homogenisation and de-gassing, the polymer solution was cast on a non-woven material (Novatexx® 2483, Freudenberg, Germany). When the preliminary evaporation of the solvent (30 s) was completed, the support with a polymer layer was transferred into the water bath to realize the polymer precipitation. Additionally, the supports were cross-linked in 0.63 wt% XDA solution in methanol for 3 days to ensure their stability in various solvents as described elsewhere [31].

The PIL-based TFC membranes were prepared using the solution casting method. Coating solutions were prepared by dispersion of the active polymer in acetone to acquire a final concentration of 4 wt%. The mixture was placed on the stirring plate and allowed to homogenise at a temperature of 25 °C. The solutions were subsequently filtered through 0.45 µm PE membrane filter, and allowed to degas overnight to avoid formation of defects. The supports were firmly fixed inside membrane casting frames to prevent the spillage of the PIL solution. Everything required for the solvent-casting procedure was placed in an airtight container with a controlled flow of nitrogen. This allowed for a degree of control, hence enabling the desired solvent evaporation rate and formation of the defect-free selective barrier. Sufficient amount of the casting solution was distributed on the surface of the support (∅50 mm) and left to solidify for at least 24 h [32].

1.5. Membrane performance evaluation

Time-lag measurements.

Single gas time-lag experiments were performed on a fixed volume / pressure increase instrument constructed by Elektro & Elektronik Service Reuter (Geesthacht, Germany) on circular samples with an effective area of 11.3 cm^2 or 2.14 cm^2. The feed gas was set at 1 bar for all the gases, and measurements at lower pressures (i.e. 0.8 bar, 0.6 bar, 0.4 bar, 0.2 bar, and 0.1 bar) were performed only for CO_2 in order to analyse the pressure dependence. The permeate pressure was measured up to 13.3 mbar with a resolution of 0.0001 mbar. The gases were always tested in the following order: H_2, He, O_2, N_2, CH_4 and CO_2, and the effective degassing was guaranteed by a turbo molecular pump. Permeabilities (Pi) are reported in Barrer (1 Barrer = $10^{-10}\cdot cm^3(STP)\cdot cm\cdot cm^{-2}\cdot s^{-1}\cdot cm\ Hg^{-1}$), and the diffusion coefficient was calculated from the so-called permeation time lag, Θ (s). The ratio of the permeability over the diffusion coefficient gives the gas solubility coefficient in its approximate form. A more detailed description of the method can be found elsewhere [33].

Scanning electron microscopy.

The morphology of TFC membranes was studied using a Hitachi N-3400 scanning electron microscope (SEM) applying an acceleration voltage of 15 kV. Samples for SEM analysis were prepared using a fracturing method from dry quick-frozen membrane segments and were sputtered with gold.

Separation performance of TFC membranes.

Mixed-gas permeation tests were performed on a high-throughput gas separation (HTGS) membrane system (HTML, Belgium) implying constant-volume variable-pressure methodology previously described elsewhere [34]. The active membrane area was 1.54 cm^2. System separation parameters were calculated based on mixed gas selectivity and permeability values. Feed gas composition was varied between

CO_2/N_2 and CO_2/CH_4 mixtures where the CO_2 partial pressure was regulated by volumetric content (15 – 85 vol%) at 5 bar feed pressure and by applying varied feed pressure (2 – 8 bar) with equimolar gas mixtures (50/50) at 26 °C. The feed gas flow rate was monitored by mass flow controllers (MFC, Bronkhorst) The driving force through the membrane was maintained constant using a vacuum pump (Pfeiffer Dua 2.5) at 4 mbar on the permeate side.

The feed and permeate gas composition were analysed by gas chromatography on a device from CGC, Interscience. The ratios between mole fractions of gas components downstream (y_i and y_j) and upstream (x_i and x_j) comprised the formula for calculating the separation factor of the membrane, $\alpha^*_{i/j}$:

$$\alpha^*_{i/j} = \frac{y_i/y_j}{x_i/x_j} \tag{1}$$

where indexes (n) i and j correspond to single gases CO_2 and N_2, respectively. Since the upstream pressure considerably exceeds the downstream pressure (vacuum) and no coupling effect between CO_2 and N_2 was observed then the intrinsic permeability selectivity approaches the separation factor [35]:

$$\alpha^*_{i/j} \approx \alpha_{i/j} \tag{2}$$

$\alpha_{i/j}$ is referred to as mixed-gas selectivity further on in the text.

The permeance Π_n (GPU) was calculated based on the rate of the pressure increase dp/dt obtained when the system has reached the steady state conditions as follows:

$$\Pi_n = \frac{V_m}{R \cdot T} \frac{V \cdot y_n}{A \cdot x_n \cdot (p_f - p_p)} \left(\frac{dp}{dt}\right) \tag{3}$$

where A is a membrane permeation area (cm^2), V is a permeation volume downstream of the membrane (cm^3), T is the operating temperature of the separation unit (K), p_f and p_p are the absolute pressure of the gas in the feed and permeate, respectively (cmHg), V_m is the molar volume of gas ($mol \cdot L^{-1}$), R is the gas constant ($L \cdot cmHg \cdot K^{-1} \cdot mol^{-1}$). p_p is considered negligible in the vacuum conditions.

3. Results and discussion

1.6. Synthesis and characterization of PILs

The functionalisation of CA yielded P[CA][Tf_2N] with an overall yield of 41 %. The reaction of the free hydroxyl groups of CA with 4-chlorobutytyl chloride was facilitated by the solubility of CA in organic solvents, which enables the formation of a homogeneous solution. P[DADMA][Tf_2N] yielded 74 % of product in the form of white solid. Its contamination with chloride anions was controlled by ionic chromatography under 400 ppm.

displays ^1H NMR spectra of CA, P[CA][Tf_2N] and P[DADMA][Tf_2N] in DMSO-d6. CA and its derivative spectra show two main sets of peaks for CA: the polymer backbone represented by the protons linked to O-linked methylene groups in the range of 5.5-3.2 ppm, and the signal of the acetyl groups in the range of 2.2-1.8 ppm [36]. The incorporation of pyrrolidinium moiety is proven by the new and isolated peak that arises at 2.99 ppm, which corresponds to the methyl group of the pyrrolidinium moiety. This signal was not coupled with any other signal of the two dimensional COSY spectrum. Additional peaks at 3.8-3.5 ppm (assigned to protons close to the charged nitrogen atom) and 2.4 ppm (assigned to protons further to the charged nitrogen atom) correspond to the new pending group.

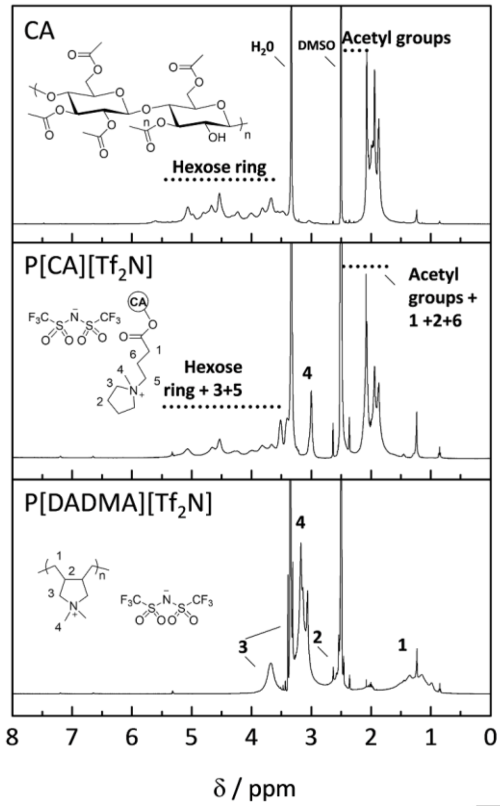

Figure 1 ^{1}H NMR (500 MHz, DMSO-d6) spectra of CA, P[CA][Tf$_2$N], and P[DADMA][Tf$_2$N].

The FTIR spectra () confirm the disappearance of the free hydroxyl groups of CA (characteristic broad stretching band at 3486 cm^{-1}) upon reaction with chlorobutyryl chloride. Also absence of the asymmetric stretching of the carbonyl group of the acetate groups (C=O) at 1736 cm^{-1}, and 1216 cm^{-1} (C-O) and 1027 cm^{-1} (C-O) confirmed this hypothesis. The successful acylation of CA to give CA-P was observed by the disappearance of the O-H, proving that the remaining hydroxyl groups of CA have reacted in the post-functionalization reaction with 4-chlorobutyryl chloride. The contribution of the new carbonyl bond should overlap with the rest of the carbonyl moieties. There are new small peaks at 780 cm^{-1} and 725 cm^{-1} and a small peak at 643 cm^{-1}, that could correspond to the stretching of C-Cl bond that should theoretically raise around 830 < 600 cm^{-1}. Once the N-alkylation and the anion exchange reactions are carried out in P[CA][Tf$_2$N], the typical peaks corresponding to the [Tf$_2$N]$^-$ anion can be observed at 1327, 1242, 1198, 1138 and 1057 cm^{-1}, showing that the anion-exchange occurred correctly. Also, the FTIR spectra of P[DADMA][Tf$_2$N] is provided, where the same peaks that correspond to the anion are observed.

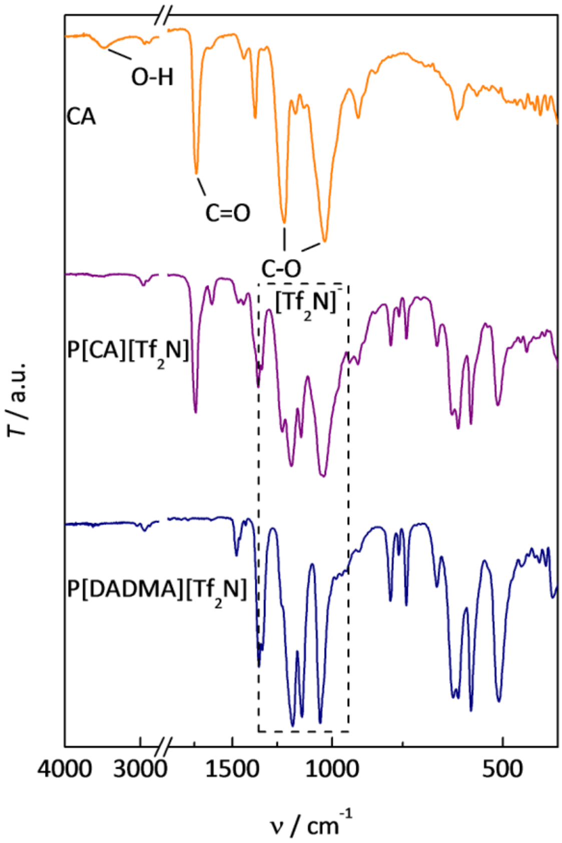

Figure 2 FTIR spectra of CA, P[CA][Tf_2N] and P[DADMA][Tf_2N].

top depicts the differential thermo-gravimetric (DTG) curves of neat CA, P[CA][Tf_2N] and P[DADMA][Tf_2N]. The latter shows the highest thermal stability, followed by CA. The incorporation of ionic groups in the CA structure lowers the maximum degradation temperature of CA from 341 °C to 288 °C, respectively. Supposedly, the ionic groups disrupt the CA packing, lowering the energy requirement to break the intra-polymer bonding and rendering the chains more labile. The higher flexibility of the polymer chains, as witnessed by the lower T_g (bottom), confirmed the reduction of intra-chain and inter-chain bonding upon functionalisation of CA. Furthermore, the presence of ionic groups may also have a catalytic effect on the backbone degradation. The same effect has been observed for CA/ILs blends [37,38]. The incorporation of the ionic moiety *via* a three-carbon atom alkyl chain linker not only decreases the thermal stability of CA, but also has a major impact on the polymer chain packing and mobility, as observed by DSC analysis.

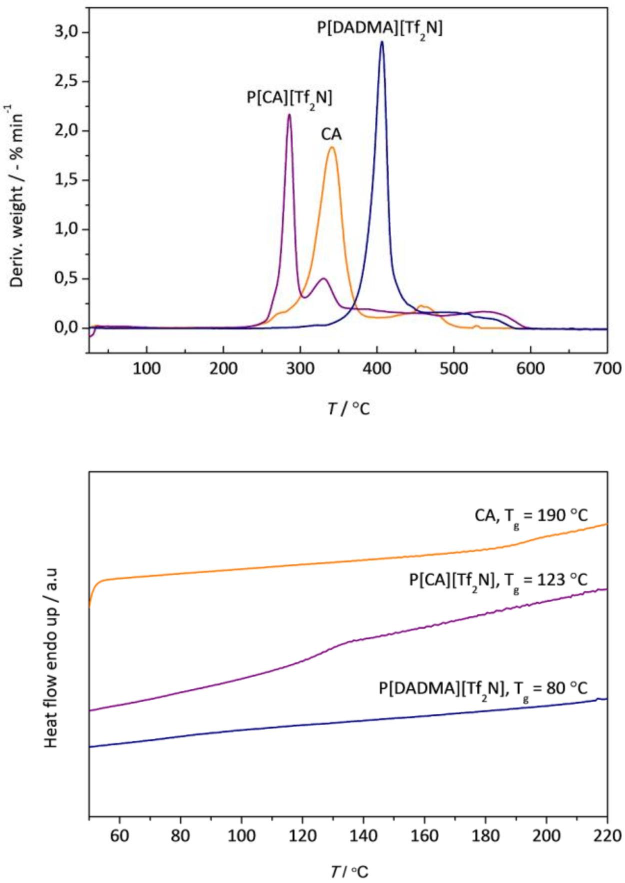

Figure 3 DTG (top) and DSC (bottom) curves (second heat run) of CA, P[CA][Tf_2N] and P[DADMA][Tf_2N] under air atmosphere recorded at 10 °C min^{-1}.

The DSC curves of the polymers (bottom) show glass transition temperatures (T_g) of CA and P[CA][Tf_2N] at 190 °C and 123 °C, respectively. This proves that the substitution of polar hydroxyl groups by ionic pending groups increases the mobility of the polymer segments, having a plasticizing effect. The backbone of P[DADMA][Tf_2N] is intrinsically more flexible, and thus this polymer has a lower T_g.

1.7. Sorption behaviour

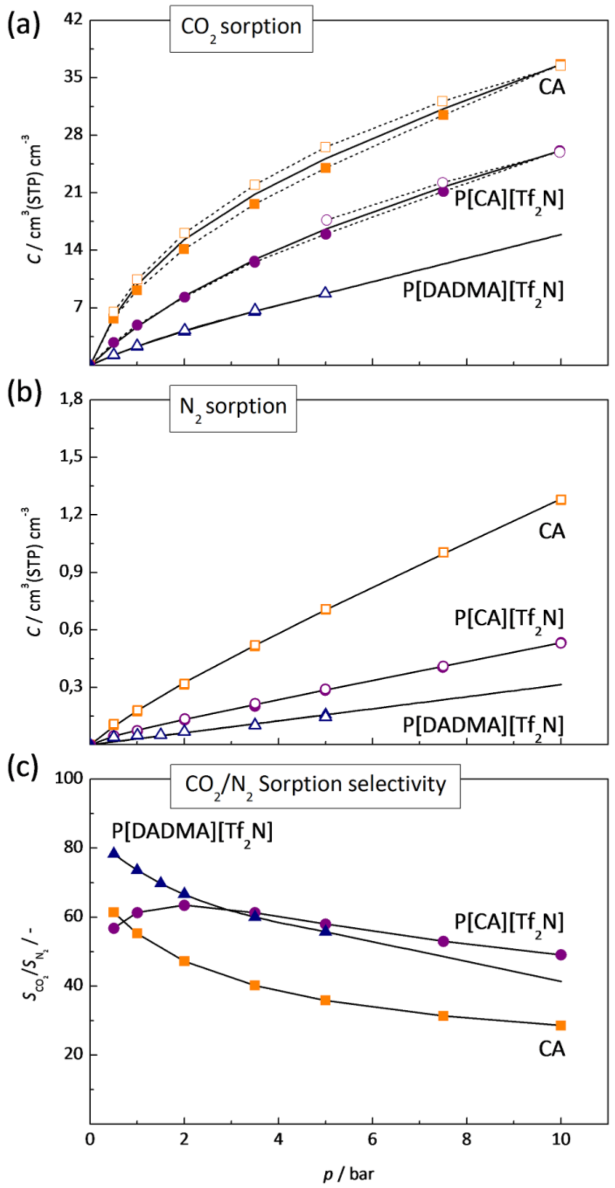

Figure 4 CO_2 (a) and N_2 (b) sorption isotherms in polymers at 20 °C. Open and filled symbols denote absorption and desorption runs, respectively. The black curves represent the simulates results based on the simple dual mode sorption model. (c) CO_2/N_2 Ideal sorption selectivity derived from single gas sorption experiments.

shows the CO_2 and N_2 sorption isotherms of P[CA][Tf_2N], CA, and P[DADMA][Tf_2N]. The CA sample has the highest CO_2 and N_2 sorption capacity among the investigated samples, while the CO_2 concentration in P[CA][Tf_2N] is twice as low compared to CA. However, the decrease in CO_2 solubility is partly compensated by a higher CO_2/N_2 solubility selectivity (by about 11.7 % at 1 bar, Table 1) due to the even lower N_2 sorption capacity.

The CO_2 sorption isotherms are strongly non-linear in the low pressure region (0 – 3 bar) and becomes roughly linear for higher pressures suggesting the dual-mode sorption mechanism (a). To describe the sorption behaviour of single gases (CO_2, N_2), experimental sorption isotherms were analysed and fitted to the dual-mode sorption model (DMM) using the non-linear regression. The sorption capacity of the polymer depends on the interaction between the polymer and the penetrant gas, and is the result of two contributions: the non-specific (C_D) sorption and the Langmuir adsorption in the polymer fractional free volume (FFV) (C_H), and equals (1) [39,40]:

$$C = C_D + C_H = k_D p + C'_H \frac{bp}{1+bp} \quad (4)$$

or may be transformed to describe the gas solubility, as follows (2):

$$S = \frac{C}{p} = k_D + C'_H \frac{b}{1+bp} \quad (5)$$

where C is the total gas concentration of penetrant in polymer (cm^3(STP)·cm^{-3}), C_D and C_H are the concentration of penetrant in the polymer matrix and micro-voids, respectively (cm^3(STP)·cm^{-3}), K_D is the Henry's law constant (cm^3(STP)·cm^{-3}·bar^{-1}), p is the gas pressure (bar), C'_H is the Langmuir saturation constant (cm^3(STP)·cm^{-3}), b (bar^{-1}) is the Langmuir affinity constant, and S is the solubility of single gas in the polymer (cm^3(STP)·cm^{-3}·bar^{-1}).

This dual-mode behaviour was most pronounced in cellulose derived samples, even though the reference P[DADMA][Tf_2N] sample exhibited a significant contribution to the non-specific sorption in FFV (1.19 cm^3(STP) cm^{-3} at 1 bar and 20 $^{\circ}$C), confirmed elsewhere [41]. The non-specific adsorption of nitrogen was much weaker at low pressures or even negligible for P[DADMA][Tf_2N]. Similarly for N_2 in P[DADMA][Tf_2N], C'_H and b are equal to zero because the experimental sorption isotherm is a straight line. Hence, these coefficients cannot be determined from Eq. (5). This case describes the situation when the total sorption is weak and the pressure is low (the equilibrium concentration changes linearly with pressure). However, in the case of P[DADMA][Tf_2N] the N_2 adsorption in FFV may be considered negligible or non-existent. This stems from the FFV in P[DADMA][Tf_2N] being much lower than that in CA and P[CA][Tf_2N] due to lower T_g, as outlined in the section 3.1. Additionally, this reduction in FFV is confirmed by the lowest Langmuir adsorption of CO_2 in P[DADMA][Tf_2N]. In summary, the total sorption capacity of N_2 follows the trend CA > P[CA][Tf_2N] > P[DADMA][Tf_2N] because both the non-specific sorption capacity and the Langmuir adsorption of N_2 decrease in this order.

For cellulose derived samples, the Langmuir adsorption dominates the total CO_2 sorption capacity (a). At 1 bar, the C_H/C ratio is equal to 81.2 % for CA and 74.3 % P[CA][Tf_2N] while being only ~50 % for sample P[DADMA][Tf_2N]. The CO_2 and N_2 adsorption in the FFV affects positively the CO_2/N_2 solubility selectivity of P[CA][Tf_2N]. Table 1 contains C_{DCO2}/C_{DN2} ratios at 1 bar, characterising the PIL matrix separation properties as rather weak in the case of CA (16.8) and moderate in the case of PILs (from 24.2 for P[CA][Tf_2N] to 37.3 for P[DADMA][Tf_2N]). A negligible (in the case of P[DADMA][Tf_2N]) or very small (cellulose derived samples) Langmuir adsorption of N_2 results in higher C_{HCO2}/C_{HN2} ratios (118-121) (b). Based on this results, P[CA][Tf_2N] exhibits intermediate CO_2 solubility selectivity in the lower pressure region exceeding the CA and P[DADMA][Tf_2N] values at higher pressures (c). Compared to the latter, this new material has still over two times better CO_2 solubility and, in relation to the neat CA, CO_2/N_2 solubility selectivity that is closer to other PILs.

Table 1 Dual-mode model parameters and separation properties obtained at 20 °C

Sample		CA	P[CA][Tf_2N]	P[DADMA][Tf_2N]
Form		powder	powder	powder
Particle diameter ($d_{v0.5}$), µm		147	331	51
CO_2 20 °C	$k_D{}^b$, [cm^3(STP) cm^{-3}·bar^{-1}]	1.85	1.21	1.12
	C'_H, [cm^3(STP) cm^{-3}]	21.15	21.07	5.31
	b, [bar^{-1}]	0.61	0.20	0.29
	Aver. relative error, [%]	4.7	3.3	1.1
	S^a, [cm^3(STP) cm^{-3}·bar^{-1}]	9.86	4.71	2.31
N_2 20 °C	k_D, [cm^3(STP) cm^{-3}·bar^{-1}]	0.11	0.05	0.03
	C'_H, [cm^3(STP) cm^{-3}]	0.21	0.05	0
	b, [bar^{-1}]	0.46	1.47	0
	Aver. relative error, [%]	2.3	2.5	6.7
	S^a, [cm^3(STP) cm^{-3}·bar^{-1}]	0.18	0.08	0.03
	$S_{CO2}/S_{N2}{}^a$	56.0	59.2	77.1
	$C_{DCO2}/C_{DN2}{}^a$	16.8	24.2	37.3
	$C_{HCO2}/C_{HN2}{}^a$	121.2	118.0	∞

[a] *at 1 bar.*

[b] *as all experimental data points lay in the non-linear sorption region the accuracy in the determination of k_D may be compromised*

1.8. Time-lag experiments

reports the CO_2 sorption isotherm in thick dense membranes at very low pressure (below 1 bar), derived from time-lag measurements assuming solution-diffusion model. The sorption capacity follows the trend P[DADMA][Tf_2N] < CA < P[CA][Tf_2N] showing that the newly synthetized PIL has the highest sorption capacity at very low pressure. This demonstrates the stronger interactions between the CO_2 and specific interaction sites in the polymer matrix of P[CA][Tf_2N] with respect to the reference polymers. However, at higher pressure or in presence of humidity, a complexation shell can be formed on the specific interaction sites, and by that, changing the overall sorption properties, and resulting in a different sorption behaviour ().

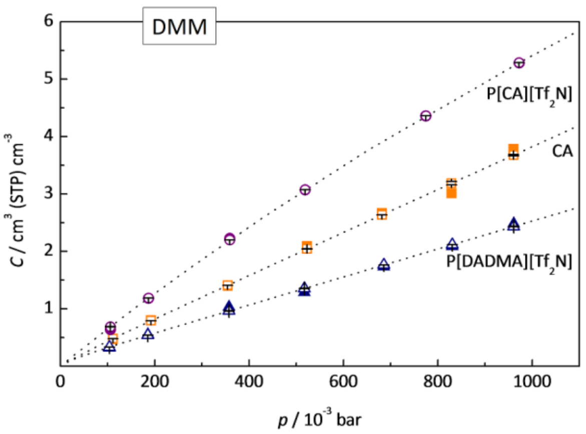

Figure 5 CO_2 sorption in thick dense membranes at pressures below 1 bar and at 25 °C. Filled and empty markers indicate experimental and calculated values, respectively. Dotted curves fit the dual-mode sorption model.

The gas transport through the dense membranes prepared by CA, P[CA][Tf_2N] and P[DADMA][Tf_2N] obeys the solution-diffusion mechanism. Table 2 **Pure gas permeability (*Px*, Barrer) and perm-selectivity (*Px/***

***PN2*), diffusion (*Dx*, 10-12 m2 s-1) and diffusion selectivity (*Dx*/*DN2*), solubility (*Sx*, cm3(STP) cm-3·bar-1) and solubility selectivity (*Sx*/*SN2*) coefficients from time-lag measurements on CA, P[CA][Tf2N] and P[DADMA]Tf2N] dense membranes measured at 1 bar and 25°C.**

Membrane	*PHe* (*PHe*/*PN2*)	*PH2* (*PH2*/*PN2*)	*PO2* (*PO2*/*PN2*)	*PCO2* (*PCO2*/*PN2*)	*PN2*	*PCH4* (*PCH4*/*PN2*)
CA	12.5 (35.8)	10.6 (30.3)	1.6 (4.7)	13.8 (39.5)	0.3	0.7 (2.1)
P[CA][Tf2N]	14.1 (42.3)	8.7 (26.1)	1.2 (3.6)	8.9 (26.8)	0.3	0.4 (1.2)
P[DADMA][Tf2N]	11.1 (30.0)	6.6 (17.7)	1.0 (2.7)	6.8 (18.4)	0.4	0.3 (0.9)
	***DHe* (*DHe*/*DN2*)**	***DH2* (*DH2*/*DN2*)**	***DO2* (*DO2*/*DN2*)**	***DCO2* (*DCO2*/*DN2*)**	***DN2***	***DCH4* (*DCH4*/*DN2*)**
CA	727 (138)	266 (50.6)	12.4 (2.36)	2.6 (0.5)	5.3	2.5 (0.47)
P[CA][Tf2N]	963 (313)	409 (133)	6.0 (1.97)	1.2 (0.4)	3.1	0.8 (0.27)
P[DADMA][Tf2N]	501 (68.3)	76.4 (10.4)	10.3 (1.41)	2.0 (0.27)	7.3	1.9 (0.26)
	***SHe* (*SHe*/*SN2*)**	***SH2* (*SH2*/*SN2*)**	***SO2* (*SO2*/*SN2*)**	***SCO2* (*SCO2*/*SN2*)**	***SN2***	***SCH4* (*SCH4*/*SN2*)**
CA	0.01 (0.26)	0.03 (0.60)	0.1 (2.0)	3.94 (79.3)	0.05	0.22 (4.3)
P[CA][Tf2N]	0.01 (0.13)	0.02 (0.20)	0.15 (1.85)	5.44 (66.8)	0.08	0.35 (4.3)
P[DADMA][Tf2N]	0.02 (0.44)	0.06 (1.7)	0.07 (1.91)	2.57 (67.8)	0.04	0.13 (3.53)

reports the permeability (*P*), diffusion (*D*) and solubility (*S*) coefficients as well as the respective ideal selectivities with respect to nitrogen (P_x/P_{N2}; D_x/D_{N2}; S_x/S_{N2}). CO_2 has a lower permeability in the two PILs than in the neat CA and follows the trend P[DADMA][Tf_2N] < P[CA][Tf_2N] < CA. The CO_2/N_2 selectivity follows the same trend. The permeability properties of the PILs are closer to the properties of typical glassy polymers. This is visible in the CO_2/He selectivity, since He permeates more than CO_2 in the PIL-based membranes, showing a clear reverse selectivity, while in CA membrane, CO_2 is more permeable than He, similar to typical rubbery polymers where the transport is “solubility controlled”. Even if no mechanical tests were performed in dry and humid condition, the effect of the humidity on the physical state of the PILs-based membranes was obvious during the sample handling. After a time-lag measurement performed in high vacuum conditions the membranes were very brittle, while they become easier to handle after some minutes of exposure to air. Hence, the humidity absorbed by the PIL matrix plasticises the polymer. This can drastically affect the permeability properties of the membrane upon the exposure to humid gases in comparison to the experiments performed under vacuum conditions.

Table 2 Pure gas permeability (P_x, Barrer) and perm-selectivity (P_x/ P_{N2}), diffusion (D_x, 10^{-12} m^2 s^{-1}) and diffusion selectivity (D_x/D_{N2}), solubility (S_x, cm^3(STP) cm^{-3}·bar^{-1}) and solubility selectivity (S_x/S_{N2}) coefficients from time-lag measurements on CA, P[CA][Tf_2N] and P[DADMA]Tf_2N] dense membranes measured at 1 bar and 25°C.

Membrane	P_{He} (P_{He}/P_{N2})	P_{H2} (P_{H2}/P_{N2})	P_{O2} (P_{O2}/P_{N2})	P_{CO2} (P_{CO2}/P_{N2})	P_{N2}	P_{CH4} (P_{CH4}/P_{N2})
CA	12.5 (35.8)	10.6 (30.3)	1.6 (4.7)	13.8 (39.5)	0.3	0.7 (2.1)
P[CA][Tf_2N]	14.1 (42.3)	8.7 (26.1)	1.2 (3.6)	8.9 (26.8)	0.3	0.4 (1.2)
P[DADMA][Tf_2N]	11.1 (30.0)	6.6 (17.7)	1.0 (2.7)	6.8 (18.4)	0.4	0.3 (0.9)
	D_{He} (D_{He}/D_{N2})	D_{H2} (D_{H2}/D_{N2})	D_{O2} (D_{O2}/D_{N2})	D_{CO2} (D_{CO2}/D_{N2})	D_{N2}	D_{CH4} (D_{CH4}/D_{N2})
CA	727 (138)	266 (50.6)	12.4 (2.36)	2.6 (0.5)	5.3	2.5 (0.47)
P[CA][Tf_2N]	963 (313)	409 (133)	6.0 (1.97)	1.2 (0.4)	3.1	0.8 (0.27)
P[DADMA][Tf_2N]	501 (68.3)	76.4 (10.4)	10.3 (1.41)	2.0 (0.27)	7.3	1.9 (0.26)
	S_{He} (S_{He}/S_{N2})	S_{H2} (S_{H2}/S_{N2})	S_{O2} (S_{O2}/S_{N2})	S_{CO2} (S_{CO2}/S_{N2})	S_{N2}	S_{CH4} (S_{CH4}/S_{N2})
CA	0.01 (0.26)	0.03 (0.60)	0.1 (2.0)	3.94 (79.3)	0.05	0.22 (4.3)
P[CA][Tf_2N]	0.01 (0.13)	0.02 (0.20)	0.15 (1.85)	5.44 (66.8)	0.08	0.35 (4.3)
P[DADMA][Tf_2N]	0.02 (0.44)	0.06 (1.7)	0.07 (1.91)	2.57 (67.8)	0.04	0.13 (3.53)

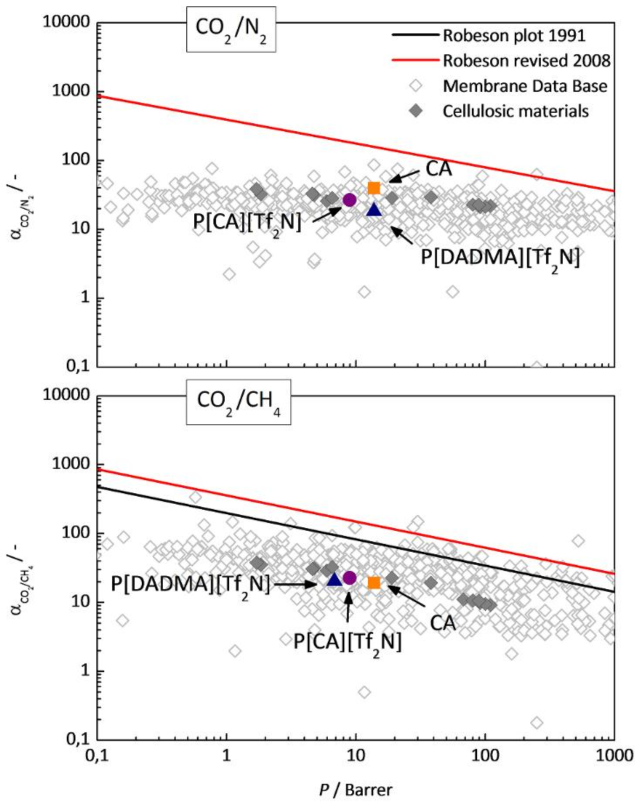

Figure 6 PILs position on the CO_2/N_2 (top) and CO_2/CH_4 (bottom) Robeson's plots. The ideal separation performance of reported membrane materials is presented for comparison and is freely available from Membrane Society of Australasia [42]**.**

The Robeson plot compares the separation performance of investigated materials and data available for CO_2/N_2 (top) and CO_2/CH_4 (bottom) gas pairs [42]. The PIL-based membranes are positioned among the central part of the plot typical for CA and CA-based materials. P[CA][Tf_2N] appears to combine the performance characteristics of CA and P[DADMA][Tf_2N].

1.9. Thin film composite membranes preparation

The porous nanofiltration supports used for membrane preparation increase simultaneously the gas permeance/flux and mechanical stability. Additionally the thin-film composite (TFC) morphology of the prepared membranes enhances the speed and the quality of separation performance evaluation. The feasibility of industrial application of prepared PILs is also determined by their capability to form a thin selective layer on top of the support.

confirms the successful preparation of TFC membranes. The defect-free selective layer can be distinguished from the support. The approximate thickness of the selective PIL layers deposited on the surface was estimated from the SEM images (), enabling the estimation of the permeability coefficients from the measured permeances.

In the case of CA-based TFC on the PI support (a), the selective polymer clearly delaminated from the support, with a total thickness of 6.2 µm. This suggests poor adhesion of CA to the support and its detachment after casting or upon fracture of the samples for SEM analysis. For the P[CA][Tf_2N] and P[DADMA][Tf_2N] samples (b, c), the separation at the interface between the PIL layer and the support is barely distinguishable, indicating the excellent adhesion between the two materials. The average thickness of the selective layer was 5.3 µm and 1.5 µm for P[CA][Tf_2N] and P[DADMA][Tf_2N], respectively. The structures of the PIL/ support-based membranes is similar in multiple identically prepared samples, confirming the high degree of reproducibility.

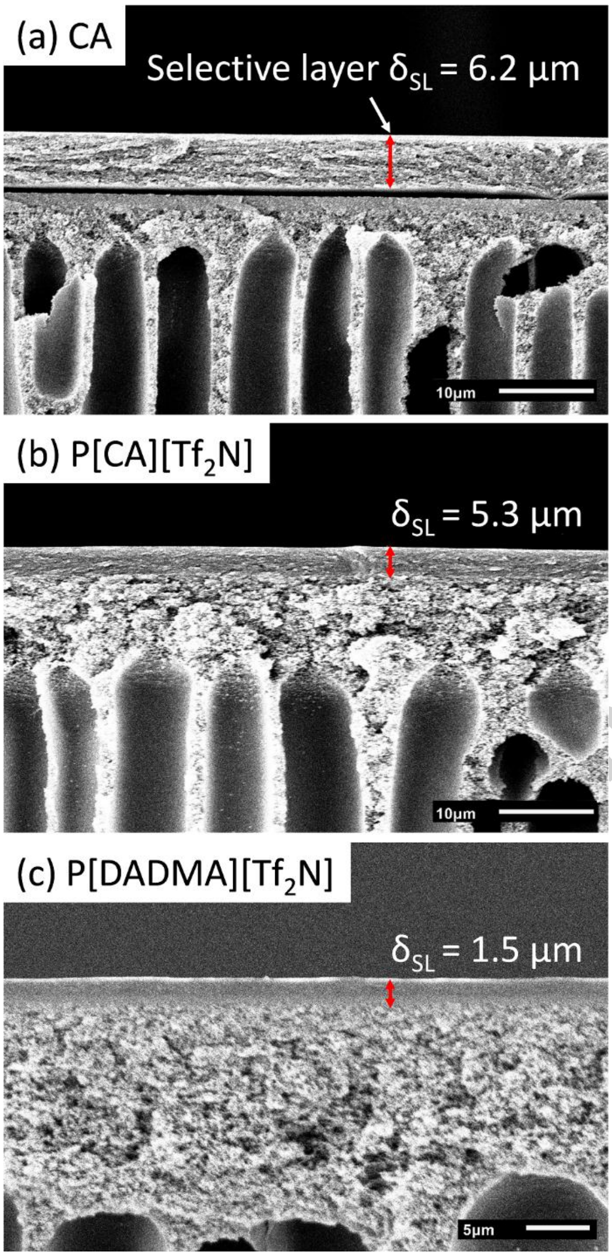

Figure 7 Cross-sectional SEM images depict the composite layered morphology of the membranes: (a) CA, (b) P[CA][Tf_2N] and (c) P[DADMA][Tf_2N]. The δ_{SL} parameter determines the average thickness of the selective layer in µm.

1.10. Mixed-gas separation

1.10. depicts how the CO_2 partial pressure in the CO_2/N_2 mixture affects the separation behaviour of the membranes. In general, CO_2 permeance (Π_{CO_2}) increases in the order CA < P[CA][Tf_2N] < P[DADMA][Tf_2N]. This order is opposite to the permeability trend shown in section 1.8.

1.10.

1.10.

The discrepancy between the dense and the TFC membranes is attributable to a higher amount of residual humidity in the mixed gas setup where the TFC membranes were tested. In the mixed gas setup, the remainder of humidity may swell or plasticize the membrane. This increases the apparent permeability of the polymer. In the mixed-gas setup, the membranes are tested with the permeate side at 4 mbar, whereas in the time-lag setup the membranes are tested at a much lower initial permeate pressure, namely 0.0001 mbar. Under these conditions the membranes are completely degassed and the ionic forces present in the P[CA][Tf_2N] make the material stiffer, decreasing the permeability.

In all cases Π_{CO_2} decreases with increasing CO_2 partial pressure, in agreement with the sorption experiments (DMS model) at pressures sufficiently low to avoid plasticisation. The main difference is that selectivity decreases, when the partial pressure of CO_2 is increased by a change in the feed composition (left), whereas selectivity increases when it is increased by a change in the absolute pressure at constant composition (right). This is the result of a delicate balance between a positive coupling effect of CO_2 and N_2 in terms of diffusion, and a negative effect on CO_2 and N_2 in terms of sorption.

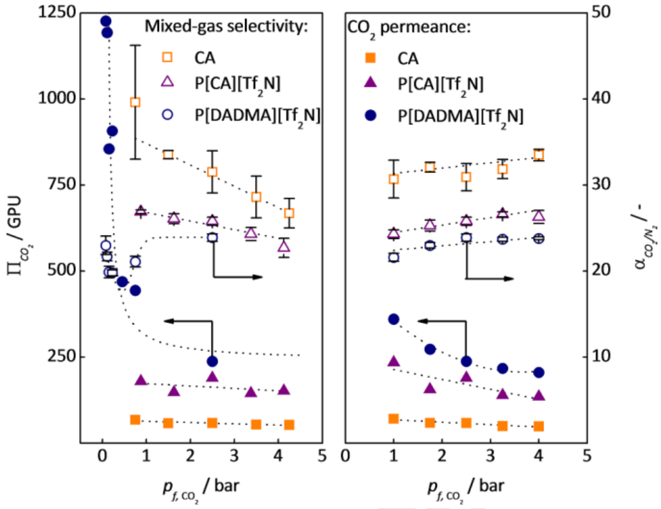

Figure 8 Increase of CO_2 partial pressure at 26 °C by (left) varying composition from 15 to 85 vol.% CO_2 at constant pressure of 5 bar, (right) changing the total pressure from 2 to 8 bar at a constant feed composition of 50/50 CO_2/N_2.

The later phenomenon is confirmed by the gas pair CO_2/CH_4 permeation experiments in P[CA][Tf_2N] (), which exhibits a more pronounced decrease in CO_2 permeance and in CO_2/CH_4 selectivity upon changing CO_2/CH_4 ratio and a stronger increase in CO_2/CH_4 selectivity upon the increase of the total pressure. Thus, all effects described for CO_2/N_2 are even stronger for CO_2/CH_4 due to both higher solubility and lower diffusivity of larger CH_4 molecules compared to N_2.

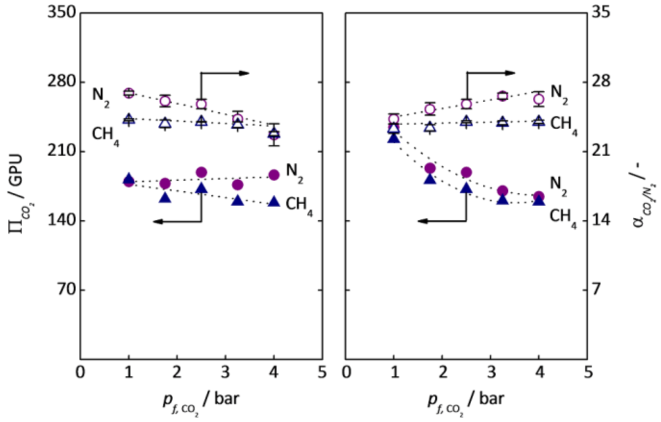

Figure 9 Role of CO_2 partial pressure in the P[CA][Tf_2N] performance at 26 °C : (left) 15 – 85 vol.% CO_2 at 5 bar feed pressure, (right) 50/50 CO_2/X feed mixture at 2 – 8 bar.

4. Conclusions

A new cellulose derived PIL was synthesized and characterized for CO_2 separation purposes. The material features several advantages: (i) the synthesis begins with the post-functionalization of a renewable, cheap and well-known industrial raw material without the need of controlled polymerization reactions; (ii) the ionic groups are covalently grafted to the polymer matrix, thus preventing them from leaching, as may occur with ILs and their blends. The incorporation of the ionic moieties in the polymer structure has led to a significant improvement (3-fold) in absolute CO_2 permeability values in comparison with neat CA under the investigated mixed gas conditions at the expense of a small decrease in selectivity. Additionally, the new material shows more stable CO_2/N_2 and CO_2/CH_4 selectivity values with increasing CO_2 content and pressure in the feed mixture, offering advantages if the membranes have to work under unstable conditions.

Acknowledgements

The financial support of this project by the European Union Seventh Framework Programme FP7/2007-2013 under grant agreement n° 608535 is gratefully acknowledged. The authors are also grateful for the financial support from the OT (11/061) funding from KU Leuven, the Belgian Federal Government through I.A.P.- P.A.I. grant (IAP 7/05 FS2), and the Polish Ministry of Science and Higher Education through International Co-financed Project grant (2978/7.PR/2014/2), as well as an Erasmus Mundus fellowship funded by EACEA (EUDIME doctoral programme 4th edition). Furthermore, the authors acknowledge Johannes Carolus Jansen (ITM-CNR) for his valuable contribution to the contents discussion.

References

[1] D. Klemm, B. Heublein, H.-P. Fink, A. Bohn, Cellulose: Fascinating Biopolymer and Sustainable Raw Material, Angew. Chemie Int. Ed. 44 (2005) 3358–3393. doi:10.1002/anie.200460587.

[2] K.J. Edgar, Edgar, K. J., Cellulose Esters, Organic, in: Encycl. Polym. Sci. Technol., John Wiley

& Sons, Inc., Hoboken, NJ, USA, 2004. doi:10.1002/0471440264.pst045.

[3] J. Puls, S.A. Wilson, D. Hölter, Degradation of Cellulose Acetate-Based Materials: A Review, J. Polym. Environ. 19 (2011) 152–165. doi:10.1007/s10924-010-0258-0.

[4] M. Mulder, Basic Principles of Membrane Technology, Second Edition 1996.pdf, Springer, 1997. http://books.google.de/books?id=tSlUcdPqnScC.

[5] S. Basu, A.L. Khan, A. Cano-Odena, C. Liu, I.F.J. Vankelecom, Membrane-based technologies for biogas separations., Chem. Soc. Rev. 39 (2010) 750–68. doi:10.1039/b817050a.

[6] D.M. D'Alessandro, B. Smit, J.R. Long, Carbon Dioxide Capture: Prospects for New Materials, Angew. Chemie Int. Ed. 49 (2010) 6058–6082. doi:10.1002/anie.201000431.

[7] R.W. Baker, K. Lokhandwala, Natural gas processing with membranes: An overview, Ind. Eng. Chem. Res. 47 (2008) 2109–2121. doi:10.1021/ie071083w.

[8] D.F. Sanders, Z.P. Smith, R. Guo, L.M. Robeson, J.E. McGrath, D.R. Paul, B.D. Freeman, Energy-efficient polymeric gas separation membranes for a sustainable future: A review, Polymer (Guildf). 54 (2013) 4729–4761. doi:10.1016/j.polymer.2013.05.075.

[9] A.L. Ahmad, Z.A. Jawad, S.C. Low, S.H.S. Zein, A cellulose acetate/multi-walled carbon nanotube mixed matrix membrane for CO2/N2 separation, J. Memb. Sci. 451 (2014) 55–66. doi:10.1016/j.memsci.2013.09.043.

[10] J. Li, S. Wang, K. Nagai, T. Nakagawa, A.W.-H. Mau, Effect of polyethyleneglycol (PEG) on gas permeabilities and permselectivities in its cellulose acetate (CA) blend membranes, J. Memb. Sci. 138 (1998) 143–152. doi:10.1016/S0376-7388(97)00212-3.

[11] W. Kim, J.S. Lee, D.G. Bucknall, W.J. Koros, S. Nair, Nanoporous layered silicate AMH-3/cellulose acetate nanocomposite membranes for gas separations, J. Memb. Sci. 441 (2013) 129–136. doi:10.1016/j.memsci.2013.03.044.

[12] J. Chen, J. Zhang, Y. Feng, J. Wu, J. He, J. Zhang, Synthesis, characterization, and gas permeabilities of cellulose derivatives containing adamantane groups, J. Memb. Sci. 469 (2014) 507–514. doi:10.1016/j.memsci.2014.06.010.

[13] C.S.K.C. Achoundong, N. Bhuwania, S.K. Burgess, O. Karvan, J.R. Johnson, W.J. Koros, Silane Modification of Cellulose Acetate Dense Films as Materials for Acid Gas Removal, Macromolecules. 46 (2013) 5584–5594. doi:10.1021/ma4010583.

[14] D. Mecerreyes, Polymeric ionic liquids: Broadening the properties and applications of polyelectrolytes, Prog. Polym. Sci. 36 (2011) 1629–1648. doi:10.1016/j.progpolymsci.2011.05.007.

[15] J. Yuan, M. Antonietti, Poly(ionic liquid)s: Polymers expanding classical property profiles, Polymer (Guildf). 52 (2011) 1469–1482. doi:10.1016/j.polymer.2011.01.043.

[16] J. Yuan, D. Mecerreyes, M. Antonietti, Poly(ionic liquid)s: An update, Prog. Polym. Sci. 38 (2013) 1009–1036. doi:10.1016/j.progpolymsci.2013.04.002.

[17] L.C. Tome, I.M. Marrucho, Ionic liquid-based materials: a platform to design engineered CO2 separation membranes, Chem. Soc. Rev. 45 (2016) 2785–2824. doi:10.1039/C5CS00510H.

[18] H. Wang, G. Gurau, R.D. Rogers, Ionic liquid processing of cellulose, Chem. Soc. Rev. 41 (2012) 1519. doi:10.1039/c2cs15311d.

[19] D.Y. Xing, N. Peng, T.S. Chung, Formation of cellulose acetate membranes via phase inversion using ionic liquid, [BMIM]SCN, As the solvent, Ind. Eng. Chem. Res. 49 (2010) 8761–8769. doi:10.1021/ie1007085.

[20] J. Tang, H. Tang, W. Sun, H. Plancher, M. Radosz, Y. Shen, Poly(ionic liquid)s: a new material with enhanced and fast CO2 absorption., Chem. Commun. (Camb). (2005) 3325–3327. doi:10.1039/b501940k.

[21] S. Zulfiqar, M.I. Sarwar, D. Mecerreyes, Polymeric ionic liquids for CO 2 capture and separation: potential, progress and challenges, Polym. Chem. (2015) 6435–6451. doi:10.1039/C5PY00842E.

[22] J.E. Bara, C.J. Gabriel, E.S. Hatakeyama, T.K. Carlisle, S. Lessmann, R.D. Noble, D.L. Gin, Improving CO2 selectivity in polymerized room-temperature ionic liquid gas separation membranes through incorporation of polar substituents, J. Memb. Sci. 321 (2008) 3–7. doi:10.1016/j.memsci.2007.12.033.

[23] K. Grygiel, B. Wicklein, Q. Zhao, M. Eder, T. Pettersson, L. Bergström, M. Antonietti, J. Yuan, Omnidispersible poly(ionic liquid)-functionalized cellulose nanofibrils: surface grafting and polymer membrane reinforcement, Chem. Commun. 50 (2014) 12486–12489. doi:10.1039/C4CC04683H.

[24] I. Garcia, I. Azcune, P. Casuso, P.M. Carrasco, H.J. Grande, G. Cabañero, D. Katsigiannopoulos, E. Grana, K. Dimos, M.A. Karakassides, I. Odriozola, A. Avgeropoulos, Carbon nanotubes/chitin nanowhiskers aerogel achieved by quaternization-induced gelation, J. Appl. Polym. Sci. 132 (2015) n/a-n/a. doi:10.1002/app.42547.

[25] S.C. Kumbharkar, R.S. Bhavsar, U.K. Kharul, Film forming polymeric ionic liquids (PILs) based on polybenzimidazoles for CO2 separation, RSC Adv. 4 (2014) 4500. doi:10.1039/c3ra44632h.

[26] L. Ansaloni, J.R. Nykaza, Y. Ye, Y.A. Elabd, M. Giacinti Baschetti, Influence of water vapor on the gas permeability of polymerized ionic liquids membranes, J. Memb. Sci. 487 (2015) 199–208. doi:10.1016/j.memsci.2015.03.065.

[27] E. Fontananova, F. Trotta, J.C. Jansen, E. Drioli, Preparation and characterization of new non-fluorinated polymeric and composite membranes for PEMFCs, J. Memb. Sci. 348 (2010) 326–336. doi:10.1016/j.memsci.2009.11.020.

[28] A.K. Hołda, I.F.J. Vankelecom, Understanding and guiding the phase inversion process for synthesis of solvent resistant nanofiltration membranes, J. Appl. Polym. Sci. 132 (2015). doi:10.1002/app.42130.

[29] P. Vandezande, X. Li, L.E.M. Gevers, I.F.J. Vankelecom, High throughput study of phase inversion parameters for polyimide-based SRNF membranes, J. Memb. Sci. 330 (2009) 307–318. doi:10.1016/j.memsci.2008.12.068.

[30] K. Vanherck, A. Cano-Odena, G. Koeckelberghs, T. Dedroog, I. Vankelecom, A simplified diamine crosslinking method for PI nanofiltration membranes, J. Memb. Sci. 353 (2010) 135–143. doi:10.1016/j.memsci.2010.02.046.

[31] K. Vanherck, P. Vandezande, S.O. Aldea, I.F.J. Vankelecom, Cross-linked polyimide membranes for solvent resistant nanofiltration in aprotic solvents, J. Memb. Sci. 320 (2008) 468–476. doi:10.1016/j.memsci.2008.04.026.

[32] D. Nikolaeva, I. Azcune, E. Sheridan, M. Sandru, A. Genua, M. Tanczyk, M. Jaschik, K. Warmuzinski, J.C. Jansen, I.F.J. Vankelecom, Poly(vinylbenzyl chloride)-based poly(ionic liquids) as membranes for CO2 capture from flue gas, J. Mater. Chem. A. 5 (2017) 19808–19818. doi:10.1039/C7TA05171A.

[33] M.R. Khdhayyer, E. Esposito, A. Fuoco, M. Monteleone, L. Giorno, J.C. Jansen, M.P. Attfield, P.M. Budd, Mixed matrix membranes based on UiO-66 MOFs in the polymer of intrinsic microporosity PIM-1, Sep. Purif. Technol. 173 (2017) 304–313. doi:10.1016/j.seppur.2016.09.036.

[34] A.L. Khan, S. Basu, A. Cano-Odena, I.F.J. Vankelecom, Novel high throughput equipment for

membrane-based gas separations, J. Memb. Sci. 354 (2010) 32–39. doi:10.1016/j.memsci.2010.02.069.

[35] J.H. Petropoulos, Mechanisms and theories for sorption and diffusion of gases in polymers, in: Polym. Gas Sep. Membr., CRC Press, 1993: pp. 17–82. books.google.it/books?id=2U9MqMG7cwkC.

[36] H. Kono, H. Hashimoto, Y. Shimizu, NMR characterization of cellulose acetate: Chemical shift assignments, substituent effects, and chemical shift additivity, Carbohydr. Polym. 118 (2015) 91–100. doi:10.1016/j.carbpol.2014.11.004.

[37] B. Lam, M. Wei, L. Zhu, S. Luo, R. Guo, A. Morisato, P. Alexandridis, H. Lin, Cellulose triacetate doped with ionic liquids for membrane gas separation, Polymer (Guildf). 89 (2016) 1–11. doi:http://dx.doi.org/10.1016/j.polymer.2016.02.033.

[38] J. Deng, L. Bai, S. Zeng, X. Zhang, Y. Nie, L. Deng, S. Zhang, Ether-functionalized ionic liquid based composite membranes for carbon dioxide separation, RSC Adv. 6 (2016) 45184–45192. doi:10.1039/C6RA04285F.

[39] R.S. Bhavsar, S.C. Kumbharkar, U.K. Kharul, Investigation of gas permeation properties of film forming polymeric ionic liquids (PILs) based on polybenzimidazoles, J. Memb. Sci. 470 (2014) 494–503. doi:10.1016/j.memsci.2014.07.076.

[40] Y. Tsujita, Gas sorption and permeation of glassy polymers with microvoids, Prog. Polym. Sci. 28 (2003) 1377–1401. doi:10.1016/S0079-6700(03)00048-0.

[41] R.S. Bhavsar, S.C. Kumbharkar, U.K. Kharul, Polymeric ionic liquids (PILs): Effect of anion variation on their CO2 sorption, J. Memb. Sci. 389 (2012) 305–315. doi:10.1016/j.memsci.2011.10.042.

[42] A. Thornton, L.M. Robeson, B.D. Freeman, CO2/N2 Gas Separation Polymers, Membr. Soc. Australas. (2012). https://www.membrane-australasia.org/polymer-gas-separation-membranes/#more-123 (accessed July 30, 2017).

Highlights

- A new class of CA-derived poly(ionic liquid) (PIL) in the form of the thin film composite (TFC) membrane was capable to separate CO_2.
- This membranes demonstrated a two-fold higher CO_2 flux compared to conventional CA in the mixed-gas permeation tests.
- The successful implementation of this membrane promotes higher permeate flows and improved process stability in a wide range of concentrations and pressures of CO2/N2 and CO2/CH4 gas mixtures.